SVU-International Journal of Engineering Sciences and Applications (2024) 5(1): 19-32
Print ISSN 2785-9967| Online ISSN 2735-4571
DOI 10.21608/svusrc.2023.237968.1150

Optimal Shape and Size of Holes in Hybrid Reinforced Concrete Beams

Sameh Yehia [1, ✉], and Arafa M. A. Ibrahim [2]
(0000-0002-5288-5627)

Abstract Hybrid reinforced concrete structures are efficient systems that include steel and fiber-reinforced polymer (FRP) reinforcement advantages, which are called fiber steel reinforced concrete (FSRC). On the other hand, passing service pipes through creating holes in reinforced concrete (RC) beams completely changes their structural behavior. Besides, RC beams with holes require rigorous nonlinear finite element (NLFE) analysis which is not typically done by design engineers. The behavior of simply-supported FSRC beams (hybrid reinforced with basalt FRP (BFRP) and steel bars) having two end holes under the effect of four-point bending loading tests was investigated. Also, NLFE models were implemented in an extensive parametric study. The studied parameters included (1) hole shapes: circular, square, and rectangular shapes; (2) height/diameter: h_o=*0.2h, 0.3h, 0.4h,* and *0.5h*; and length: L_o=*0.3h, 0.5h, 0.7h,* and *1.0h (h: overall beam depth)*. Compared to a similar beam without holes, the holes produce reductions of up to 53%, 44%, 85%, 64%, and 58% in the beam's cracking load, ultimate strength, absorbed energy, post-cracking stiffness, and post-yield stiffness, respectively (the lowest in cases of circular holes). In order to obtain the beneficial behavior of FSRC beams, it is recommended to drill the beam with a hole size diameter of up to *0.4h* and up to a hole size length of *0.3h* for square holes. On the contrary, the effect of hybrid reinforcement gains less significant enhancement in the case of the rectangular holes.

Keywords: Optimal Holes, Finite Element Model, FRP, Hybrid Reinforcement, Design Recommendations.

1 Introduction

One of the causes of deterioration in steel-reinforced concrete (SRC) buildings is corrosion of steel reinforcement **[1-3]**. In addition to the complete disruption in the building during restoration and treatment of the damaged reinforced concrete (RC) members due to steel corrosion, the owners of these buildings incur huge sums of money to carry out the repair works and restore the functions of those members. Fiber-reinforced polymer (FRP) composites are an effective alternative to reinforcing steel, especially in harsh environmental conditions because of their corrosion resistance, high strength, and lightweight. The lack of ductility of concrete members reinforced with FRP composites alone has motivated those interested in this field to combine both the steel and FRP reinforcement in RC structures, and the resulting reinforced system is called hybrid FRP-steel RC (FSRC) members. On the other hand, in modern and industrial RC buildings, there is ever increasing need for holes at different positions of structural elements. These holes enable the continuous use of ducts and pipes for sanitation, electricity, telephone and computer networks, heating, ventilation, and air conditioning.

The most feasible alternative solution may be pass these ducts via transverse holes in the floor beam rather than placing them underneath the soffit of the beam, which must be covered by a suspended ceiling, leaving a "dead space" in each level. Despite the promising solutions offered by FSRC beams with holes in structural engineering, especially in multistory buildings, there are no code provisions and design guidelines for such beams.

In the past few decades, several research efforts have been conducted toward understanding the structural behavior and the controlling parameters of FSRC systems. For example, some studies **[4-6]** showed that the FSRC systems are more deformable than the SRC systems. The relevant results showed that, by adding the steel bars, the flexural ductility of the hybrid members could be improved, and the crack width decreased compared with beams reinforced with FRP bars. In another study **[7]**, it was emphasized that the flexural performance of concrete beams is enhanced by combining both the steel and glass FRP (GFRP) bars. Based on large numerical investigations **[8]**, it was concluded that the steel and FRP bars in FSRC beams are responsible for the flexural capacity and the ductility of the beams, respectively. Therefore, the smaller ratios of FRP to steel reinforcement (A_f/A_s) were reported to give enhanced ductility. Similarly, the investigations of another study **[9]**

Received: 20 September 2023/ Accepted: 9 October 2023
Corresponding Author, E-mail
✉Sameh Yehia, dsyehia@hotmail.com / s.yehia@suezuni.edu.eg
1. Civil Engineering Department, Faculty of Engineering, Suez University, Egypt
2. Civil Engineering Department, Faculty of Engineering, South Valley University, Egypt

showed that the deflection and the maximum crack width of the FSRC beams significantly increase with the increase in the A_f/A_s ratio, and the deformability index of the FSRC beams reduces as the A_f/A_s increases. Furthermore, from the steel corrosion's point of view, it was reported that by providing the FRP bars in the corners or near the outer surface of the concrete sections, the durability of the FSRC beams is improved **[7, 10-11]**. To give design guidelines, through experimental investigations on FSRC beams **[12]**, it was recommended to design such beams to fail due to FRP rupture or concrete crushing following the steel yielding. Extending from this, based on extensive finite element (FE) investigations **[13]**, it was concluded that the FSRC beams should be designed with over-reinforcement to give higher flexural capacity and stiffness as well as adequate ductility. In this case, the ratio of A_f/A_s should be ranged from 1 to 2.5. The results also showed that to meet the economic targets, the beams may be designed with under-reinforcement with A_f/A_s to be more than 1.0. In another attempt to apply the hybrid reinforcing systems, experimental investigations were carried out on FSRC girders **[14]**, and the results recommended a range for the A_f/A_s ratio to be from 1.0 to 2.33 to prevent the early rupture of FRP bars and enhance the post-yield strength as well as stiffness. For RC beams with holes, the structural performance has been addressed in many studies **[15-26]**. The common conclusions of these studies were as follows: (1) the presence of holes in SRC beams alters their simple behavior to a more complex one; i.e., the corners of the hole are subjected to the high-stress concentration that leads to early cracking and causes relative reductions in the strength and stiffness of the beam and (2) the effect of holes on the structural behavior of the beams depends on many parameters including the shape and size of the holes, the location of the holes concerning both the span and depth of the beams, the loading type, the compression and tension reinforcement ratios, and the type and configurations of the strengthening schemes around the holes. Regarding the holes' shape, it was emphasized that holes with sharp corners have a major effect on the strength, stiffness, and deformability of the beams, and holes with circular or semicircular shapes have less effect **[27]**. Further studies **[28, 29]** concluded that the structural performance of SRC beams with holes is more sensitive to both the hole size and hole proximity to the supports, and it is slightly influenced by the steel reinforcement ratio. In this context, the investigations of finite element analysis **[30]** found that the effect of circular holes on the cracking and ultimate strengths is significant when the hole's diameter exceeds one-third of the beams' depth. Also, the holes were classified according to their influence on the structural behavior of RC beams into small and large holes; e.g., a circular hole is considered large if its diameter (d_o) exceeds $0.4d$, while the square hole is large if its edge length (L_o) exceeds $0.25d$, where d is the effective depth of the beam **[30 and 31]**. Results of recent investigations **[32]** confirmed the mentioned classification, where the presence of circular holes with $d_o < 0.4d$ causes small changes in the cracking and ultimate loads, while holes with larger diameters produced premature cracking and significantly reduced the strength.

Recently, basalt FRP (BFRP) composites have been suggested as a promising alternative to GFRP **[33]**. Indeed, Basalt fibers were proven to be non-toxic and non-ignitable as well as ecologically amenable. Besides, it is green material, produced from natural basalt rock. In summary, BFRP has several good mechanical and durability properties and great performance in different temperature conditions and harsh environments. Consequently, BFRP composites have been utilized in different experimental and numerical studies as well as practical applications. E.g., through experimental and numerical investigations, BFRP composites have been proposed as seismic-resistant reinforcement **[34 and 35]**. The findings of the aforementioned tests demonstrated that using both BFRP composites and steel reinforcements ensures the necessary post-earthquake recoverability, allowing for the reduction of residual column deformation and the regulation of post-yield stiffness.

Based on the mentioned above, the authors of this research are currently working on a specialized research project on FSRC beams with openings. The project started with an extensive experimental and numerical program on many FSRC beams reinforced with hybrid reinforcement of steel and BFRP bars with and without holes **[36 and 37]**. The studied holes were rectangular and of a fixed size. This program also touched on the study of strengthening the holes internally using steel or BFRP bars and externally using BFRP sheets. The findings emphasized the significant effect of the holes on both the strength and serviceability of the beams and proposed an effective way to restore a large percentage of the beam strength capacity due to the presence of the holes by combining both the internal reinforcement and the external strengthening.

In order to extend the findings of the previous studies, there is still a crucial need to investigate the effect of various parameters on the structural performance of such beams. Based on the confirmed reliability of the developed three-dimensional (3D) finite element (FE) model that was created using ANSYS code version 15 **[38]** and verified in the previous study of the authors **[37]**, an extensive FE parametric study presented here to appropriately define the effect of both the shape and size of the holes on the different characteristic levels of the structural response of the beams. Indeed, the objective of this section is to extend and enhance the discussion of the previous studies and obtain design recommendations for FSRC beams with holes. The first section of the research reviews the details of the FE model. In contrast, the second section discusses the results of fifteen FE models created to address the effect of both the shape and size of

the holes on the structural performance of the beams in terms of strength, stiffness, serviceability, and deformability limits.

2. Design and Description of the Analyzed Beams

As mentioned earlier, the authors performed several experimental tests on FSRC beams with and without rectangular holes. In the current numerical study, the solid experimentally tested FSRC beam (BSF) from **[37]** was employed as a reference beam for the numerical parametric study. As shown in **Fig. 1**, the beam was simply supported over a clear span of 1800 mm and a total length of 2000 mm, and was tested under a four-point flexural static loading setup. The beam had a rectangular cross-section of 150 mm in width and 300 mm in total depth. The concrete beams were designed to be manufactured using normal strength concrete of a target cubic compressive strength of 35 MPa, 10 mm diameter steel and BFRP bars used as main reinforcement, and 8 mm diameter steel stirrups. Based on the results of some preliminary laboratory tests, the mechanical properties of all types of reinforcement were determined and are summarized in **Table 1**.

Table 1 Mechanical properties of reinforcing bars of the experimental beams **[37]**

Material type	Elastic modulus E (GPa)	Yield stress f_y (MPa)	Tensile strength f_u (MPa)
Φ 10 mm steel bars	200	480	610
φ 8 mm steel stirrups	200	270	380
Φ 10 mm BFRP bars	48.1	-	1113

2.1. Design of the Flexural Reinforcements

By reviewing the existing literature related to the conditions of choosing the reinforcement ratio of FRP RC (FRC) beams and FSRC beams and their relationships with the failure modes of the beams **[1-14]**, it may be concluded that two types of reinforcement ratios may be associated to FSRC beams; namely: over-reinforced and under-reinforced conditions. In general, if the beam is reinforced with an effective hybrid reinforcement ratio, ρ_{eff}, determined by **Eq. 1 [12]** more than the balanced reinforcement ratio, ρ_b, determined by **Eq. 2 [39]** (i.e., $\rho_{eff} > \rho_b$), the beam is being over-reinforced and the flexural failure is expected to be due to crushing of concrete before rupture of FRP bars. If $\rho_{eff} < \rho_b$, the beam is under-reinforced and the FRP bars are ruptured before the concrete crushing.

$$\rho_{eff} = \rho_s \frac{f_y}{f_{fu}} + \rho_f \quad \textbf{(1)}$$

$$\rho_b = 0.85\beta_1 \frac{f_c'}{f_{fu}} \frac{E_f \varepsilon_{cu}}{E_f \varepsilon_{cu} + f_{fu}} \quad \textbf{(2)}$$

where ρ_s and ρ_f are the steel and FRP reinforcement ratios, respectively; f_y and f_{fu} are the yield strength of steel bars and the ultimate strength of FRP bars, respectively; E_f is the modulus of elasticity of FRP reinforcement; f_c' and ε_{cu} are the concrete compressive strength and the crushing strain of concrete (0.003), respectively; and f_y is the equivalent rectangular stress block depth to the neutral axis depth ratio. Here in this study, the FRP reinforcement ratio was chosen as one third of the total reinforcement ratio (i.e., $\rho_f = (\rho_s+\rho_f)/3$), and an iterative procedure was applied to choose suitable number of steel and BFRP bars having diameters of 10 mm. Following the condition of over-reinforced beams, it was decided to reinforce the beams with two steel bars and one BFRP bar giving a value of $\rho_{eff} = 1.8\ \rho_b$. (i.e., $\beta_1 = 0.85$).

2.2. Design of the Shear Reinforcements

Based on the flexural design and after choosing the tension reinforcements of the beam, the ultimate flexural strength was predicted based on the design recommendations of **[40]**. Following to that the shear reinforcement was designed based on the design procedure of **[40]** with excessive amounts in order for preventing shear failure of the beam. Therefore, the shear reinforcement consisted of 8-mm-diameter steel stirrups arranging every 150 mm along the beam length, giving a value for the shear strength equals approximately 170% of the flexural strength. The following **Fig. 1** shows the Geometrical and reinforcement details of the reference beam.

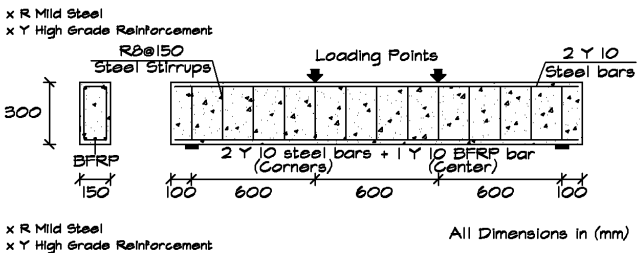

Fig. 1. Geometrical and reinforcement details of the reference beam **[37]**.

2.3. Parametric Study

The investigated parameters include:

(1) Hole shape: circular, square, or rectangular; and
(2) Hole size: the height (or the diameter) of the holes ranged from *0.2h* to *0.5h* while the length ranged from *0.2h* to *0.7h*, where *h* is the total depth of the beam.

Fig. 2 illustrates the geometry and details of the holes used in the numerical parametric study. The parametric study was carried out on a simply supported beam that was very similar to the one pre-tested by the authors **[36]** (**Fig. 1**). Dimensions and reinforcement details, material

properties, and loading scheme followed exactly the experimental data. As shown in **Table 2**, the 3D FE models included a total of 15 beams. Among the modeled beams; one beam was tested without a hole to serve as a reference beam, four beams have two circular holes with different diameters, four beams have two square holes with different edge sizes, and the other six beams have two rectangular holes with different lengths and different heights.

The identification code for model No. 1 in **Table 2** (BSF) defines the reference FSRC beam without holes, while the other codes define the beams with holes. The symbols CO, SO, and RO define the cases of circular holes, square holes, and rectangular holes, respectively. The symbols in parentheses express the size of the holes as follows: In the cases of circular and square holes, the hole size is a single value that expresses the size of the hole in relation to the depth of the beam, while in the case of rectangular holes, the hole size is expressed by two values in the form of (*height * length*), and each of them is relative to the total depth of the beam. For example, BSF-CO(*0.2h*) represents a beam having circular holes with a diameter of *0.2h*, BSF-SO(*0.2h*) represents a beam having square holes with an edge length of *0.2h*, and BSF-RO(*0.3h*0.5h*) represents the case of rectangular holes with height and length of *0.3h* and *0.5h*, respectively.

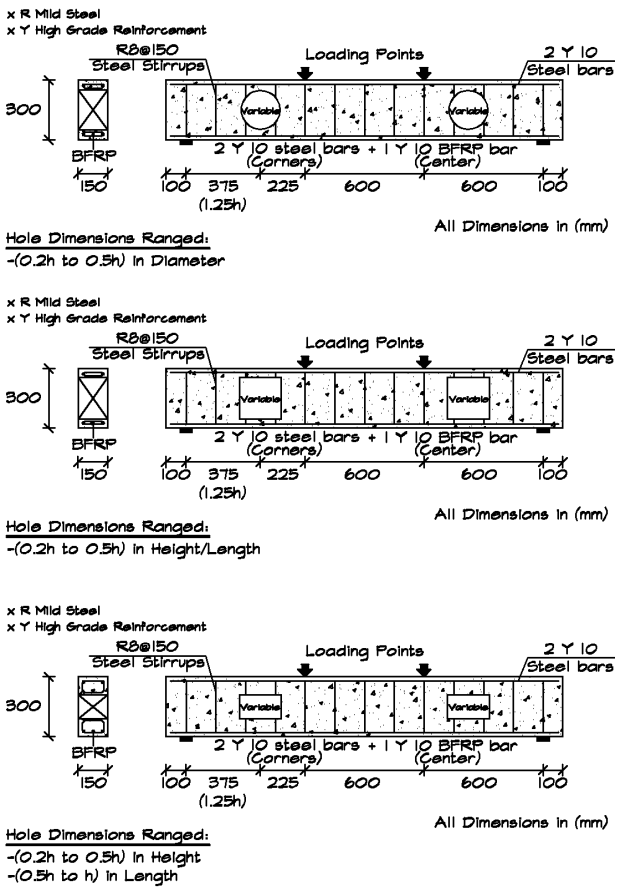

Fig. 2. Geometrical and reinforcement details of the beams used in the numerical investigations.

Table 2 Details of models used in the numerical parametric study

Model No.	ID	Tension Reinforcement			Hole parameters (refer to **Fig. 2**)			
		A_s (mm^2)	A_f (mm^2)	A_f/A_t	Shape	h_o or d_o (mm)	L_o (mm)	S_o (mm)
1	BSF	157.00	78.50	0.33	-	-	-	-
2	BSF-CO (*0.2h*)				Circular	60	-	300
3	BSF-CO (*0.3h*)					90	-	
4	BSF-CO (*0.4h*)					120	-	
5	BSF-CO (*0.5h*)					150	-	
6	BSF-SO (*0.2h*)				Square	60	60	
7	BSF-SO (*0.3h*)					90	90	
8	BSF-SO (*0.4h*)					120	120	
9	BSF-SO (*0.5h*)					150	150	
10	BSF-RO (*0.3h*0.5h*)				Rectangular	90	150	
11	BSF-RO (*0.3h*0.7h*)					90	210	
12	BSF-RO (*0.3h*h*)					90	300	
13	BSF-RO (*0.2h*0.7h*)					60	210	
14	BSF-RO (*0.4h*0.7h*)					120	210	
15	BSF-RO (*0.5h*0.7h*)					150	210	

3. Numerical Models

3.1. General Overview

This section describes the developed finite element modeling using the software package **ANSYS version 15 [38]**. All the necessary steps to create the models that were prepared to investigate the behavior of reinforced concrete beams having rectangular holes under a four-point flexural loading scheme were explained in detail and the steps taken to generate the successive stages of the numerical load-deformation response and the failure criteria of the beams were also discussed. The above-described experimental test data was adopted to verify the developed FE models. Owing to the beam's symmetry in both the longitudinal and transverse directions, only quarters of the beams, as shown in **Fig. 3**, were modeled. Symmetric boundary conditions were applied to the beam's center planes along the longitudinal and transverse directions. The relevant constraints in the node points of the finite element were used to depict these planes of symmetry. This method drastically decreased the amount of time needed for computation and the

amount of disc space needed. The discretization and meshing size were chosen with a maximum aspect ratio of three **[41]**, respecting the locations of reinforcing bars, holes, and loading and support plates. The numerical finite element modeling of the experimental beams was built considering the material, geometrical, and contact nonlinearities between the reinforcing bars and concrete. Furthermore, appropriate element types and material models were carefully chosen in order to simulate the behavior of each component of the model according to what has been applied in previous studies, found in the literature **[34 and 42]**.

3.2. Modelling of Concrete

A three-dimensional solid element was utilized to model the solid concrete components of the beams (Solid65). This element has eight nodes with three orthogonal translational degrees of freedom at each node. The element has also the capabilities of cracking in three orthogonal directions, and crushing of concrete, in addition to the capability of plastic deformation. The creation of a model for concrete behavior is a difficult task because concrete has varied behavior in compression and tension. To simulate the concrete, the linear isotropic and multi-linear isotropic material properties under compression, together with the tensile behavior and several other concrete material parameters, must be defined. In this study, the cubic compressive strength of concrete was taken from the experimental data (i.e., f_{cu} = 35 MPa), giving an equivalent cylinder strength (f_c' = 28 MPa).

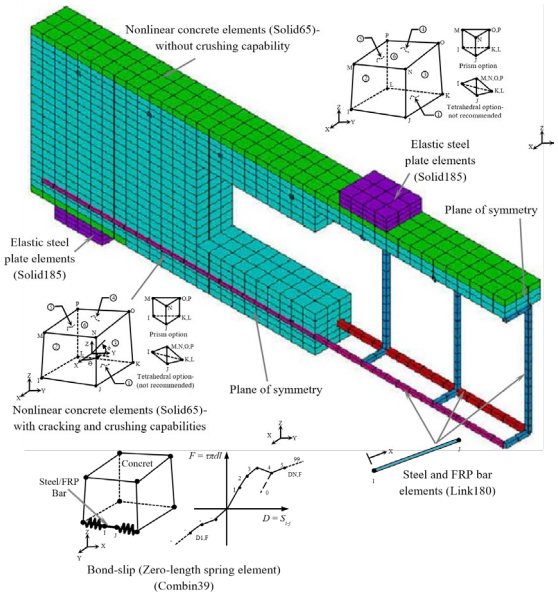

Fig. 3. Details of the FE model and element types.

The uniaxial compressive stress-strain relationship for concrete (**Fig. 4.a**) was defined using the MacGregor model **[43]** through **Eq. 3**, as follows.

$$f = \frac{E_c.\varepsilon}{1+\left(\frac{\varepsilon}{\varepsilon_o}\right)^2} \quad \textbf{(3)}$$

Where: f = stress at any strain ε, ε_o= strain at the ultimate compressive strength f_c' (ε_o = 2 f_c'/E_c), and E_c is the modulus of elasticity of concrete.

Owing to the convergence problems that come from the stress concentration at the locations of loads and supports, it was decided to model the concrete elements adjacent to the loading and supporting plates while neglecting the crushing capability. As for the behavior of concrete in tension, the model by **[44]** (**Fig. 4.a**), which was adopted in many research studies **[43]** and also recommended by ANSYS was used here in this study. Through this model, the tensile behavior still increases linearly up to the maximum tensile strength of (f_t = 0.62($\sqrt{f_c'}$) before dropping to 60 % of the maximum strength, followed by a descending behavior up to the zero strength corresponding to a strain equals six times that at the ultimate strength. For concrete, the Poisson's ratio was taken to be 0.2. The cracking face conditions are represented by the shear transfer coefficient β_t. The value of β_t typically falls between 0.0 and 1.0, where 0.0 indicates a smooth crack (complete loss of shear transfer) and 1.0 indicates a rough crack (no loss of shear transfer) **[38]**. Using the findings of **[45]**, the shear transference coefficients for open and closed cracks were calculated. When the open crack's shear transfer coefficient dropped below 0.2, convergence issues developed. After some effort, the right values for the open and closed shear coefficients were determined to be 0.4 and 0.9, respectively.

3.3. Modelling of Steel and BFRP Reinforcements

In the current work, both the steel and BFRP reinforcement were modelled using the discrete technique employing the 3D spar LINK180 element in order to extract the internal strains in the reinforcement bars and maintain their proper locations. Translations in the x, y, and z directions are possible at each of the two nodes of this element. The element also has plastic deformation capabilities. Using the von Mises yield criterion and a strain-hardening ratio of 0.01 **[45]**, the material model for steel bars was assumed to be bilinear isotropic as shown in **Fig. 4.b**, while the uniaxial elastic brittle material model was used for BFRP bars up to rupture.

In the present study, in order to obtain the internal strains in the reinforcement bars and keep them in their right positions, the discrete technique using the 3D spar LINK180 element was followed to model both the steel and BFRP reinforcement. This element has two nodes with three degrees of freedom – translations in the x, y,

and z directions. The element is also capable of plastic deformation. As shown in **Fig. 4.b**, the material model for steel bars was assumed to be a bilinear isotropic, based on the von Mises yield criterion, with a strain-hardening ratio of 0.01 **[45]**, while the uniaxial elastic brittle material model was applied for the BFRP bars up to rupture. Both steel and BFRP reinforcement were expected to have the same mechanical characteristics as those discovered during the experimental tests. Steel reinforcement and BFRP reinforcement were given assumed Poisson's ratios of 0.3 and 0.2, respectively.

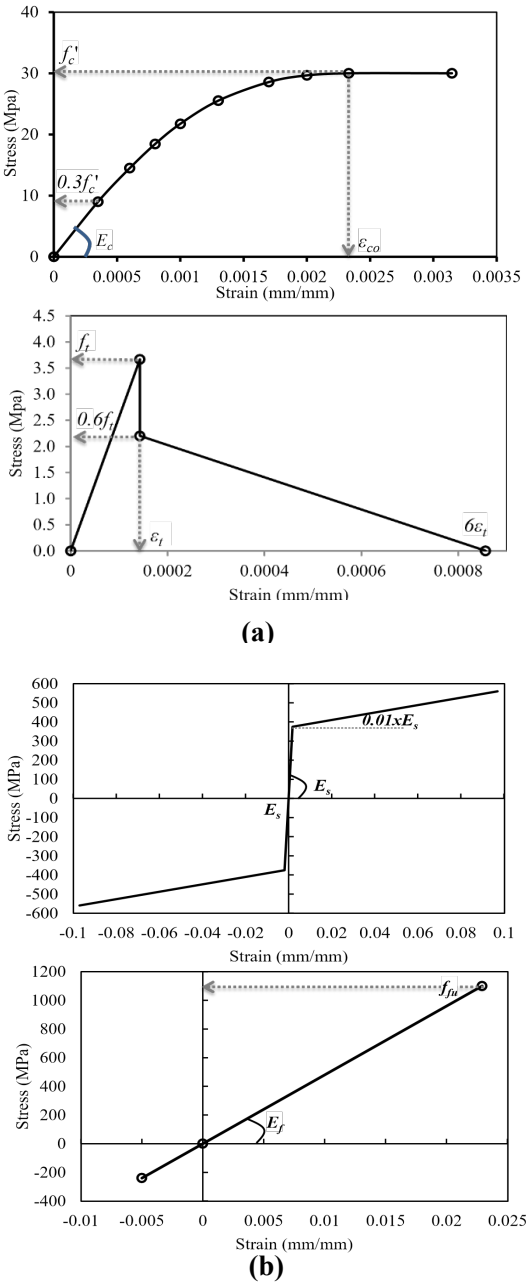

Fig. 4. Constitutive material models of: (a) concrete in compression and tension and (b) steel and BFRP bars.

3.4. Modelling of Steel Plates

SOLID185 elements are used to simulate the steel plates at the supports for the beams. There are eight nodes in this element, each with three degrees of freedom for translations in the x, y, and z axes. With the exception of its resistance to crushing and cracking, this element's definition is essentially identical to that of the SOLID65 element. With an elastic modulus of 200,000 MPa and a Poisson's ratio of 0.3, it was believed that the steel plates would act in an elastic manner.

3.5. Modeling of Bond-Slip Behavior

The previous experimental and numerical studies of the authors **[34 and 46]** showed great influence on the bonding behavior of reinforcing bars and recommended various bond-slip models of BFRP bars depending on their surface conditions. Therefore, it was very necessary to include the bond-slip models in the current FE models to accurately simulate the performance of the tested specimens. To consider the bonding behavior between the steel and BFRP bars and the surrounding concrete, the zero length-spring element COMBIN39 was adopted in this study with the aid of the bond-slip model of BFRP bars developed by the authors in a previous study **[34]** and of steel bars recommended in CEB-Code model **[47]**. **Fig. 5** shows the bond-slip models for both the 10-mm-diameter deformed steel and BFRP bars.

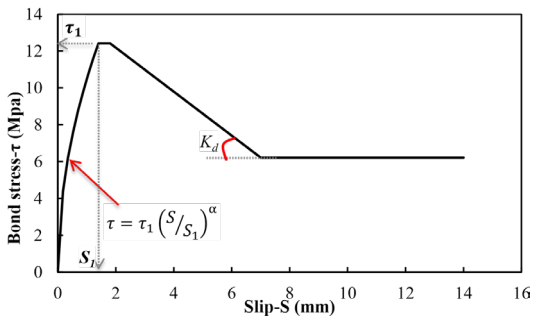

Fig. 5. Bond-slip models of steel **[45]** and BFRP bars **[34]**.

3.6. Modeling of Loading and Boundary Conditions

Where there are supports and loadings, as well as points of symmetry, beam boundary conditions must be used. The model in use is symmetric around the central planes of the beams. The nodes that cross these symmetry planes must be restrained to only point in perpendicular directions. These nodes, therefore, have degrees of freedom constraints of UX = zero and UZ = zero at the middle planes in the longitudinal and transverse directions, respectively. Similarly, proper boundary conditions were applied at the supports to simulate the same conditions of the experimental beams. Moreover, the nodes in the transverse direction at the loading line were given a coupling degree of freedom in the Y-direction in order to displace together with the same value.

3.7. Non-Linear Solution and Failure Criteria

The total load applied in this investigation was divided into a series of load steps or increments. Iterations of Newton-Raphson equilibrium deliver convergence within tolerance bounds at the end of each load increase. The ANSYS program's automatic time stepping anticipates and regulates the load step sizes for which the maximum and lowest load step sizes are necessary. The number of load steps and the lowest and maximum step sizes were established after numerous attempts. The loads were applied gradually with lower load increments during the concrete cracking, steel yielding, and final stages. Each model's failure was noted when the solution did not converge.

4. Results of the Numerical Investigations and Discussion

Fig. 6 proposes a structural performance model (i.e., *P-Δ* curve, where *P* and *Δ* are the total load and mid-span deflection, respectively) for the FSRC beams with and without holes. Through this model, the structural performance consisted of three zones as follows: (1) the pre-cracking zone which ends by the first cracking point (P_{cr} and Δ_{cr}), (2) the post-cracking zone with a stiffness of K_1 ends at the yielding of steel bars (P_y and Δ_y); and (3) hardening zone up to the peak point (P_m and Δ_m), with stiffness of K_2, before failure of the beams. **Table 3** summarizes the values of both the load and deflection of the characteristic points of the described model for the numerically studied beams and the effects of the investigated parameters on the load-deflection curves are shown in **Fig. 7**.

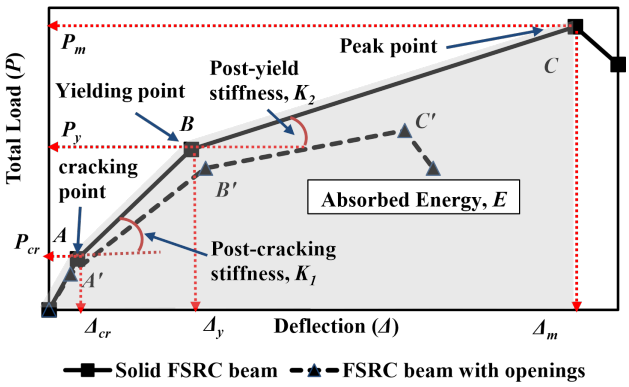

Fig. 6. Structural performance model for FSRC beams with and without holes.

Table 3 Results of the numerical investigations

No.	ID	P_{cr} (kN)	First Cracking Position	P_y (kN)	Δy (mm)	P_m (kN)	Δ_m (mm)	ε_{fm} (%)	Failure Mode
1	BSF	27.4	Mid-span	69.3	4.0	133.7	30.1	2.14	CC
2	BSF-CO (*0.2h*)	23.9	Mid-span	70.2	4.3	129.1	31.3	2.05	CC
3	BSF-CO (*0.3h*)	23.6	Mid-span	68.6	4.3	125.5	30.4	2.01	CC
4	BSF-CO (*0.4h*)	23.2	Mid-span	69.0	4.5	115.8	28.1	1.69	SO
5	BSF-CO (*0.5h*)	22.4	Mid-span	73.2	5.4	102.3	24.6	1.20	SO
6	BSF-SO (*0.2h*)	25.7	Mid-span	68.5	4.3	125.2	29.4	2.00	CC
7	BSF-SO (*0.3h*)	25.1	Mid-span	68.9	4.5	121.4	28.8	1.87	CC
8	BSF-SO (*0.4h*)	18.5	Hole	69.7	5.1	105.2	25.1	1.24	SO
9	BSF-SO (*0.5h*)	15.0	Hole	NA	NA	73.4	20.4	0.36	SO
10	BSF-RO (*0.3h*0.5h*)	22.2	Hole	78.2	6.9	105.0	23.9	1.39	SO
11	BSF-RO (*0.3h*0.7h*)	17.4	Hole	69.6	5.5	84.5	20.1	0.68	SO
12	BSF-RO (*0.3h*h*)	13.7	Hole	68.9	8.4	75.4	11.6	0.41	SO
13	BSF-RO (*0.2h*0.7h*)	20.1	Mid-span	68.7	5.1	103.0	24.9	1.25	SO
14	BSF-RO (*0.4h*0.7h*)	13.0	Hole	73.1	11.1	76.8	14.6	0.41	SO
15	BSF-RO (*0.5h*0.7h*)	11.4	Hole	NA	NA	53.7	10.6	0.21	SO

Note: CC is the failure due to concrete crushing and SO is the shear failure at hole zone.

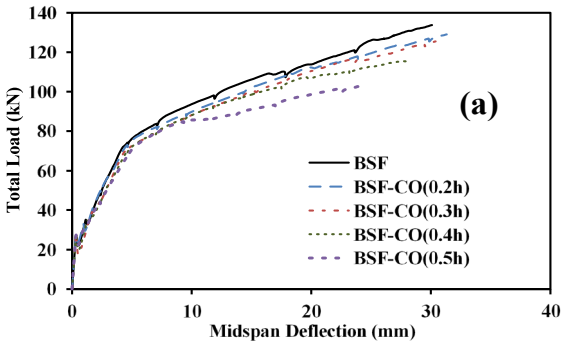

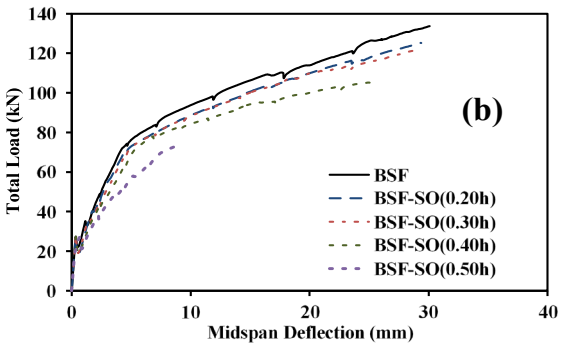

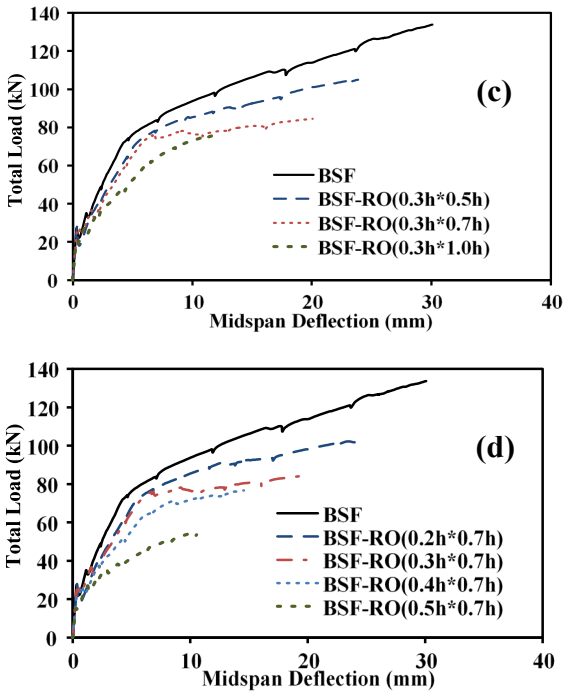

Fig. 7. Effect of the investigated parameters on the load-deflection curves of the beams: (a) effect of circular holes' diameter, (b) effect of square holes' edge size, (c) effect of rectangular holes' length, and (d) effect of rectangular holes' height.

4.1. General Behavior and Failure Modes

Referring to **Table 3**, it is obvious that the first cracking of the solid beam, all beams with circular holes, and beams with small square and rectangular holes (i.e., defined here as the square holes that have edge length less than *0.4h* or the rectangular holes that have a height less than *0.3h*)) were flexural cracking at locations of the maximum tension fibers (mid-span sections). The first cracking of all other beams was diagonal shear cracks created at the lowest corners of the holes near the supports. Regarding the failure modes, it was noticed that the solid beam failed due to the crushing of concrete at locations of maximum compression fibers (i.e., CC defined when $\varepsilon_c > 0.003$) before the rupture of the BFRP bar. The presence of holes with relatively small sizes (e.g., circular and square with diameter or edge length less than *0.4h*) did not alter the failure mode of the beams, while the presence of the other holes altered the failure to another one that resulted from the concentration of the stresses around the holes (SO), as presented in **Table 3** and **Fig. 8**.

In conjunction with the failure modes, the strain levels of BFRP bars at failure of all beams were also recorded and summarized in **Table 3**. Also, **Fig. 9** shows the effect of the investigated parameters on the BFRP strain ratio at failure (i.e., ε_{fm} / ε_{fu}; where ε_{fm} and ε_{fu} are the induced BFRP strain at failure and the rupture BFRP strain, respectively). In general, the strain level of the BFRP bar of beams with holes at failure is smaller than that of the counterpart solid beams. The presence of holes with a circular diameter or square edge lengths less than *0.4h* resulted in a minor decrease in the FRP strain at failure, compared with the solid beams. With an additional increase in the size of the holes, more reduction in the BFRP strain ratio was observed. For example, the presence of circular holes with diameters of *0.4h* and *0.5h* resulted in FRP strain ratios of 70% and 50%, respectively. The ratios induced in beams with square holes with edge lengths of *0.4h* and *0.5h* were 52% and 15%, respectively. While maintaining the height of the holes, the contribution of BFRP reinforcement to increasing the bearing capacity of the FSRC beams decreases sharply with increasing the length of the holes. For example, the BFRP bar was able to reach 80% of its rupture strain with holes of length equal to *0.3h*, while this ratio decreased to about 58% and 17% with holes of lengths equal to *0.5h* and *1.0h*, respectively. A similar effect was observed for the holes' height; i.e., by maintaining the holes' length, the BFRP bar was able to reach 52%, 30%, and 9% of its rupture strain with holes of height equal *0.2h*, *0.3h*, and *0.5h*, respectively.

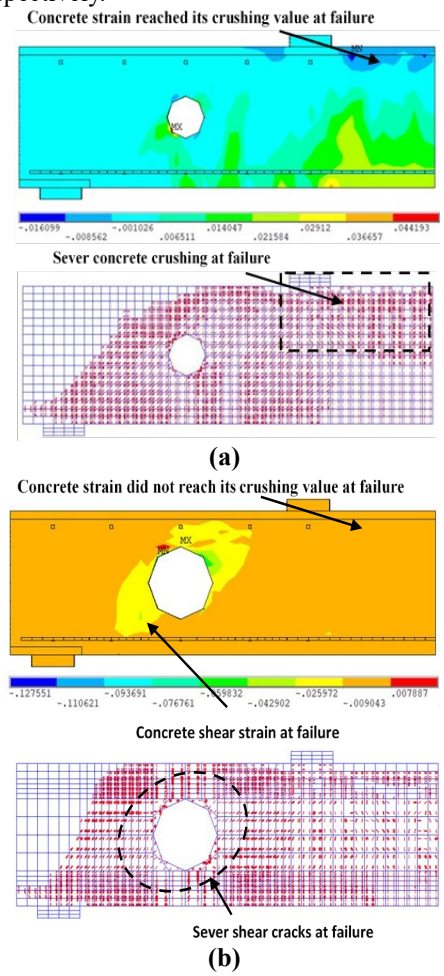

Fig. 8. Common failure patterns of the modeled beams: (a) failure due to concrete crushing (CC) and (b) failure due to diagonal shear at hole (SO).

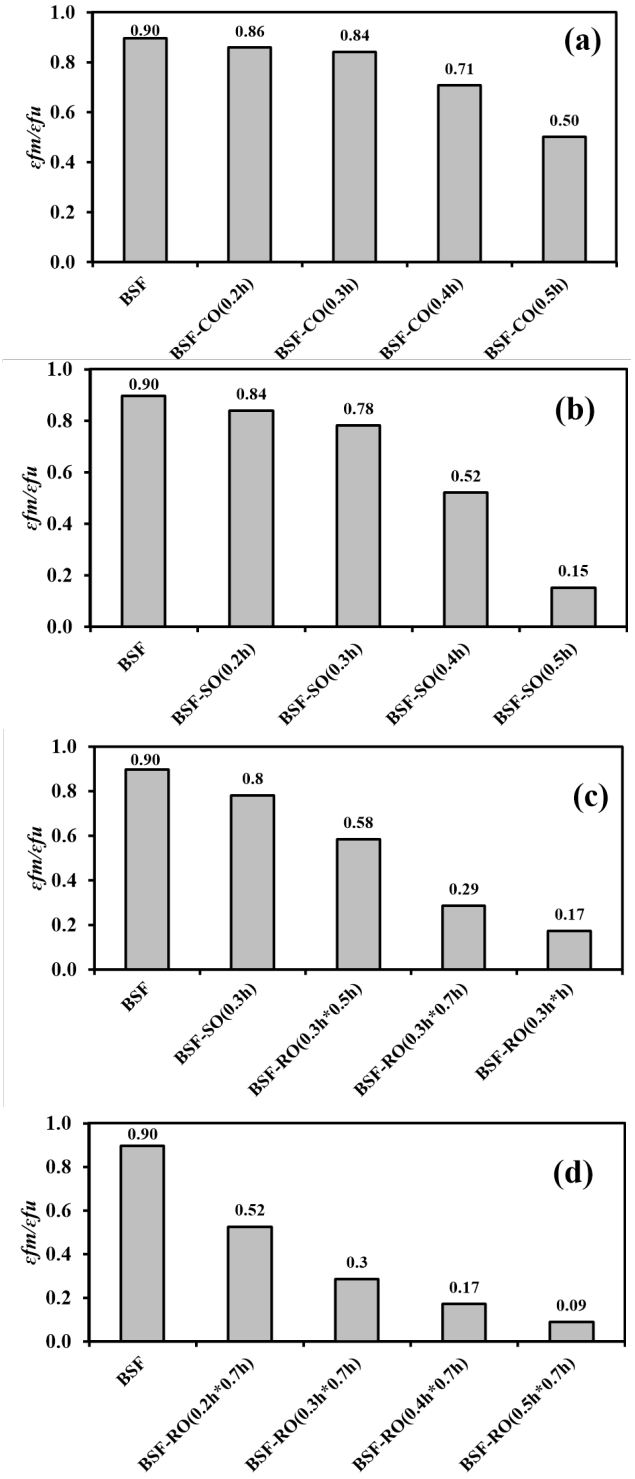

Fig. 9. Effect of the investigated parameters on the ratio of BFRP strain at failure to the rupture strain, $\varepsilon_{fm}/\varepsilon_{fu}$: (a) beams of circular holes with different diameters, (b) beams of square holes with different edge sizes, (c) beams of rectangular holes with different lengths, and (d) beams of rectangular holes with different height.

4.2. Cracking and peak loads

Table 3 lists the cracking and peak loads obtained from the FE modeling of the beams and **Fig. 10** gives the effect of the investigated parameters on the relative cracking and peak loads. In this figure, the relative cracking and peak loads represent the ratios of the cracking and peak loads of the beams with holes to that of the beams without holes, respectively. It is clear that the presence of holes in the beams significantly reduces their cracking and peak loads. The percentage decreases in the cracking and peak loads ranged from 1% to 58% and 3% to 60%, respectively. The presence of circular holes with diameters less than 40% of the overall beam depth did not cause a significant decrease in both the cracking and peak loads of the beams, while increasing the diameter of the holes to 50% of the beam depth resulted in decreases of about 18% and 24% in the cracking and peak loads, respectively. Holes with sharp corners, on the other hand, had the greatest effect. For instance, the percentage reductions in the cracking load due to the presence of square holes having edge lengths of *0.4h* and *0.5h* were 33% and 45%, respectively, while the corresponding values in the peak load were 21% and 46%, respectively. Furthermore, by keeping the holes' length the same, by increasing the holes' height from *0.2h* to *0.5h* the relative cracking and peak loads decreased from 74% to 42% and from 77% to 40%, respectively. Similarly, by increasing the holes' length from *0.3h* to *h* the relative cracking and peak loads decreased from 90% to 50% and from 90% to 44%, respectively.

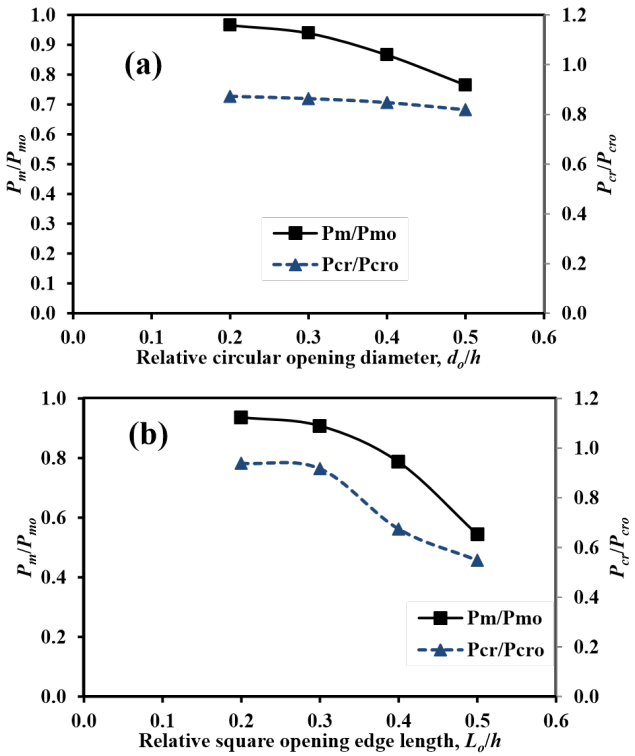

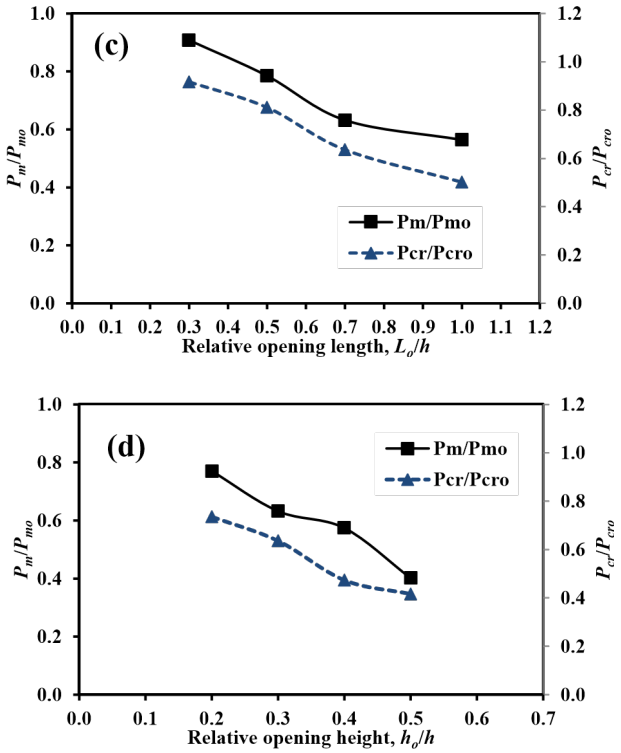

Fig. 10. Effect of the investigated parameters on the relative cracking and failure loads: (a) beams of circular holes with different diameters, (b) beams of square holes with different edge sizes, (c) beams of rectangular holes with different lengths, and (d) beams of rectangular holes with different heights.

4.3. Post-cracking and post-yielding stiffness

It has been confirmed in past studies that before yielding the main longitudinal steel reinforcement, FRP bars have a smaller elastic stiffness and in turn a slight contribution to the flexural deformations of the beams, compared with the steel bars. In the post-yielding stage, however, the hardening behavior of the beams, which is represented by the post-yield stiffness, greatly depends on the contribution of the FRP reinforcement. Also, it is well known that the stiffness of flexural members greatly depends on the moment of inertia of its cross-section. Keeping in mind the aforementioned facts, the impact of the investigated parameters on both the pre-yielding (post-cracking) stiffness (K_1) and the post-yielding stiffness (K_2) were analyzed. Definitions of the two indices are as follows: (**Eq. 4** & **Eq. 5**)

$$K_1 = (P_y - P_{cr}) / (\Delta_y - \Delta_{cr}) \quad \textbf{(4)}$$

$$K_2 = (P_m - P_y) / (\Delta_m - \Delta_y) \quad \textbf{(5)}$$

The values of both stiffness indices are summarized in **Table 4** for all modeled beams. The effect of the investigated parameters on the beam's stiffness was evaluated using two stiffness indices as follows: the relative pre-yielding stiffness (k_1/k_{1o}), where k_1 and k_{1o} are the pre-yielding stiffness of the beams with and without holes, respectively; and the relative post-yielding stiffness (k_2/k_{2o}), where k_2 and k_{2o} are the post-yielding stiffness of the beams with and without holes, respectively. The effect of the investigated parameters is presented in **Fig. 11**. Referring to the presented results, it is observed that the height of the hole is the most influencing parameter on both the relative pre-yielding and post-yielding stiffness, compared with the effect of other parameters; i.e., this state confirmed the relationship between the stiffness and moment of inertia. E.g., the increase in the holes' height from *0.2h* to *0.4h* decreased the values of k_1/k_{1o} and k_2/k_{2o} from 0.88 to 0.48 and from 0.7 to 0.44, respectively. On the other hand, the effect of holes' length was more pronounced on the post-yield stiffness and only a slight effect was noted on the pre-yielding stiffness. By approximately duplicating the holes' length, the values of k_1/k_{1o} and k_2/k_{2o} were reduced by approximately 95% and 50%, respectively. Moreover, holes with circular shapes had the lowest impact on the two stiffness indices.

Table 4 Effect of the investigated parameters on the stiffness, ductility, and absorbed energy of the modeled beams

No.	ID	$K_1 = (P_y - P_{cr}) / (\Delta_y - \Delta_{cr})$ (kN/mm)	$K_2 = (P_m - P_y) / (\Delta_m - \Delta_y)$ (kN/mm)	$\mu_m = \Delta_m / \Delta_y$ (mm/mm)	E (kN.mm)
1	BSF	11.45	2.47	7.5	3069.3
2	BSF-CO (*0.2h*)	11.41	2.18	7.3	3040.2
3	BSF-CO (*0.3h*)	11.27	2.18	7.1	2855.6
4	BSF-CO (*0.4h*)	10.82	1.98	6.2	2524.1
5	BSF-CO (*0.5h*)	9.82	1.52	4.5	1995.3
6	BSF-SO (*0.2h*)	10.77	2.26	6.9	2742.2
7	BSF-SO (*0.3h*)	10.41	2.16	6.4	2642.3
8	BSF-SO (*0.4h*)	10.53	1.78	4.9	2055.3
9	BSF-SO (*0.5h*)	6.67	NA	NA	441.3
10	BSF-RO (*0.3h*0.5h*)	8.46	1.58	3.5	1937.8
11	BSF-RO (*0.3h*0.7h*)	9.89	1.02	3.6	1388.6
12	BSF-RO (*0.3h*h*)	6.72	2.04	1.4	620.0
13	BSF-RO (*0.2h*0.7h*)	10.09	1.73	4.9	2022.3
14	BSF-RO (*0.4h*0.7h*)	5.49	1.08	1.3	856.5
15	BSF-RO (*0.5h*0.7h*)	4.07	NA	NA	424.9

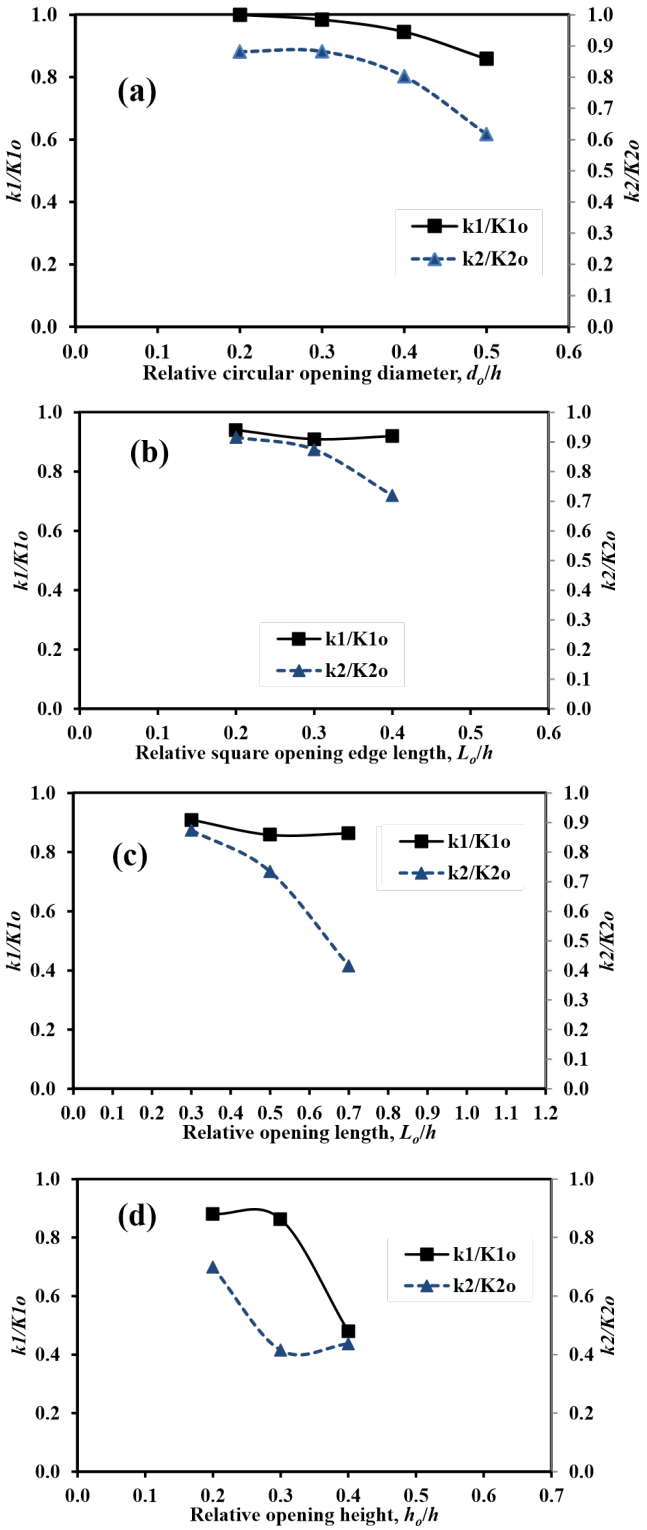

Fig. 11. Effect of the investigated parameters on the relative post-cracking and post-yield stiffness: (a) beams of circular holes with different diameters, (b) beams of square holes with different edge sizes, (c) beams of rectangular holes with different lengths, and (d) beams of rectangular holes with different heights.

4.4. Ductility and absorbed energy

Besides the strength and stiffness indices, both the relative displacement ductility (μ_m/μ_{mo}) and the relative absorbed energy (E/E_o) were evaluated here to address the influence of the investigated parameters on the deformability of the beams. The displacement ductility is defined as the ratio of the displacement at peak load to that at the steel yielding (i.e., $\mu_m = \Delta_m / \Delta_y$) and the absorbed energy is defined by the area under the load-deflection curve, as shown in **Fig. 6**. **Table 4** lists the values of the displacement ductility and the absorbed energy of the modeled beams and **Fig. 12** gives the effect of the investigated parameters on the relative ductility (i.e., μ_m/μ_{mo}, where μ_m and μ_{mo} are the ductility of the beams with and without holes, respectively) and the relative absorbed energy (i.e., E/E_o, where E and E_o are the absorbed energy of the beams with and without holes, respectively). Referring to **Table 4** and **Fig. 12,** it is clear that the presence of holes in FSRC beams resulted in maximum reductions in the relative ductility by 57% and 89%, respectively, and maximum reductions in the relative absorbed energy by 82% and 86%, respectively. It has also been observed that rectangular and square holes had the greatest effect on the two deformability indices, and their effect increases clearly with the increase in either their depth or length.

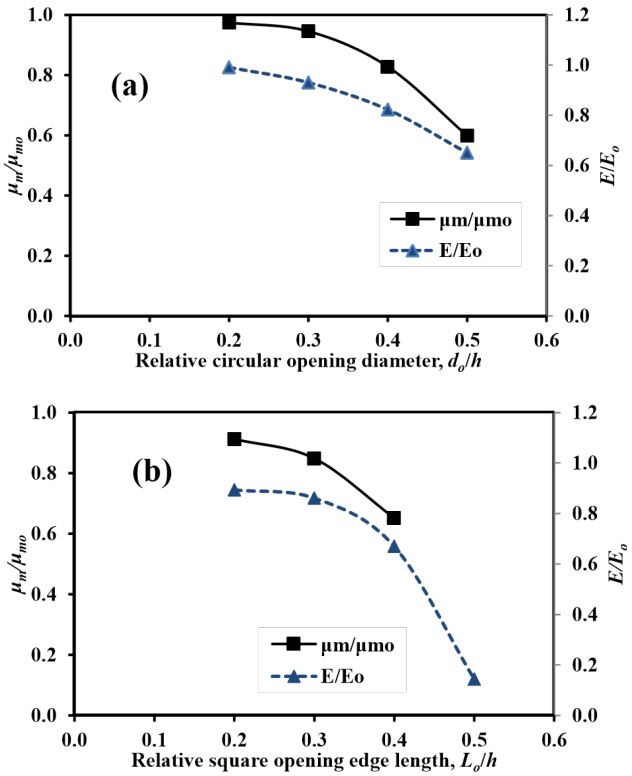

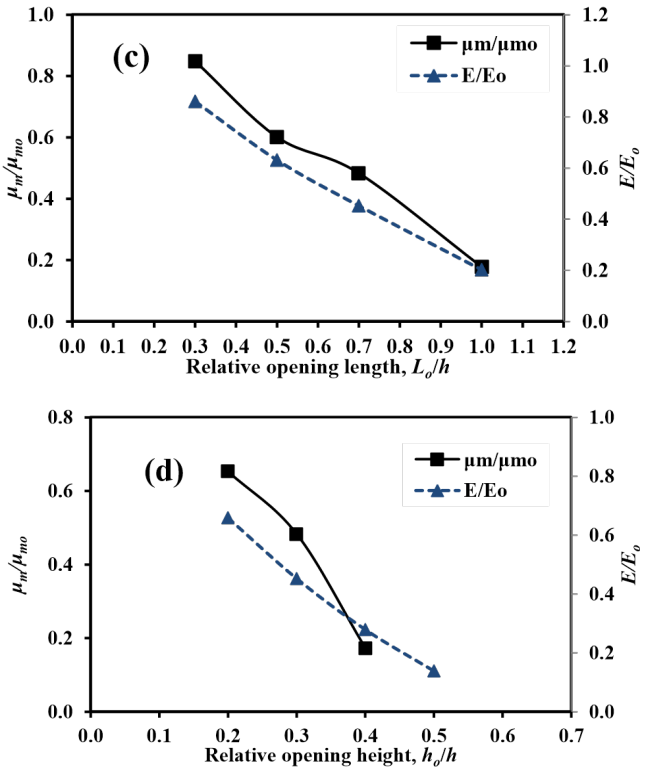

Fig. 12. Effect of the investigated parameters on the relative ductility and absorbed energy: (a) beams of circular holes with different diameters, (b) beams of square holes with different edge sizes, (c) beams of rectangular holes with different lengths, and (d) beams of rectangular holes with different heights.

5. Conclusions

This research aimed to give insight into the effect of holes on the strength, stiffness, and serviceability limit states of concrete beams reinforced with BFRP and steel bars (FSRC beams). From the FE analysis and within the scope of the present investigations, the following findings could be drawn:

1. The presence of holes leads to a decrease in cracking and ultimate strengths, post-cracking and post-yield stiffness, and ductility and absorbed energy of FSRC beams. The amount of reduction is greatly affected by the hole shape, hole height, and hole length.

2. Crack patterns and failure modes of the beams depend also on the shape and size of the holes. The presence of square or rectangular holes with a height or length > *0.2h* results in earlier cracks at the hole location. These cracks increase in number and propagate continuously with the increase in applied load and lead to earlier failure compared to similar beams without holes. On the other hand, the cracks of beams with circular holes having a diameter of up to $d_o = 0.5h$ initiate at mid-span (positions of flexure zone) and continue to propagate until later failure. At any particular load, both the number of cracks and the beam deflection increase with the increase in hole size.

3. The presence of holes limits the effectiveness of BFRP reinforcement in increasing both the strength and post-yield stiffness of FSRC beams. For instance, while the maximum BFRP strain at failure for a solid FSRC beam reaches about 90% of the rupture strain, it reaches almost 9% in the counterpart beam with rectangular holes of height $h_o = 0.5h$. The reduction amount in the maximum BFRP strain at failure, and hence the contribution of BFRP reinforcement in the FSRC system, are highly proportional to both the shape and size of the holes.

4. The maximum reductions in the cracking and failure load range from 6% in beams with holes of height, $h_o = 0.2h$, to 60% in beams with holes of $h_o = 0.5h$, the corresponding reductions in the post-cracking and post-yield stiffness range from 5% to 64% and from 8% to 55%, respectively, and the corresponding reductions in the ductility and absorbed energy range from 9% to 83% and from 11% to 86%, respectively.

5. In beams with circular holes, an increase in the holes' diameter from $d_o = 0.3h$ to *0.5h* causes increases of 5%, 20%, 30%, and 12% in the reductions of cracking load, failure load, absorbed energy, and post-cracking stiffness, respectively. The corresponding values in beams with square holes due to the increase of the hole's edge size from $L_o = 0.3h$ to *0.5h* are 40%, 42%, 84%, and 36%, respectively.

6. Circular holes are much better than those with sharp corners. For circular holes with diameters of $d_o > 0.4h$, it is extremely recommended to provide special reinforcement around the holes to restore the strength of the beams.

7. For beams with square holes, it is not recommended to apply holes with edge lengths more than 0.3 of the beam's depth unless special reinforcements are provided around the holes.

8. Hybrid reinforcement significantly affects the behavior of beams with holes. Furthermore, after steel reinforcement yielding, the BFRP bars increase the maximum load of the beam up to 93% for beams without holes. Moreover, the maximum load of the beam with circular holes increased by 84% in the case of a hole size diameter of *0.2h* and by 83% in the case of a hole size length of *0.2h* for square holes. Also, by increasing the hole size, the gain increases decreased. On the contrary, the effect of hybrid reinforcement doesn't gain the desirable performance, and the increase in the maximum load was 34% in the case of the lowest rectangular holes' size (*0.3h*0.5h*).

References

[1] H. T. Zhu, S. Z. Cheng, D. Y. Gao, S. M. Neaz, and C. C. Li, "Flexural behavior of partially fiber reinforced high-strength concrete beams reinforced with FRP bars,", *J Construct Build Mater.*, vol. 161, pp. 587–597, 2018.

[2] P. Escórcio and P. M. França, "Experimental study of a rehabilitation solution that uses GFRP bars to replace the steel bars of reinforced concrete beams," *J Eng Struct*., vol. 128, pp. 166– 183, 2016.

[3] J. Xia, W. L. Jin, and L. Y. Li, "Effect of chloride-induced reinforcing steel corrosion on the flexural strength of reinforced concrete beams," *Mag Concr Res*., vol. 64, pp. 471–85, 2012.

[4] D. Y. Yoo, N. Banthia, and Y. S. Yoon, "Flexural behavior of ultra-high-performance fiber reinforced concrete beams reinforced with GFRP and steel rebars,", *J Engineering Structures*, vol. 111, pp. 246-262, 2016.

[5] W. Ge, J. Zhang, D. Cao, and Y. Tu, "Flexural behaviors of hybrid concrete beams reinforced with BFRP bars and steel bars," *J Construction and Building Materials*, vol. 87, pp. 28-37, 2015.

[6] D. Lau and H. J. Pam, "Experimental study of hybrid FRP reinforced concrete beams,", *J Engineering Structures*, vol. 32, pp. 3857-3865, 2010.

[7] W. Qu, X. Zhang, and H. Huang, "Flexural behavior of concrete beams reinforced with hybrid (GFRP and steel) bars," *J Compos. Constr.*, vol. 13, pp. 350-359, 2009.

[8] Bui LVH, Stitmannaithum B, Ueda T, "Ductility of concrete beams reinforced with both fiber-reinforced polymer and steel tension bars", *J Advanced Concrete Technology* 16: 531-548, 2018.

[9] X. Ruan, C. Lu, K. Xu, G. Xuan, and M. Ni, "Flexural behavior and serviceability of concrete beams hybrid-reinforced with GFRP bars and steel bars," *J. Composite structures,* vol. 235, pp. 111772, 2020.

[10] H. Y. Leung and R. V. Balendran, "Flexural behaviour of concrete beams internally reinforced with GFRP rods and steel rebars," *J Struct Survey*, vol. 21, pp. 146–57, 2003.

[11] A. Acciai, A. D'Ambrisi, M. De Stefano, L. Feo, F. Focacci, and R. Nudo, "Experimental response of FRP reinforced members without transverse reinforcement: failure modes and design issues," *J Compos B Eng*., vol. 89, pp. 397–407, 2016.

[12] A. El Refai, F. Abed, and A. Al-Rahmani, "Structural performance and serviceability of concrete beams reinforced with hybrid (GFRP and steel) bars," *J Construction and Building Materials*, vol. 96, pp. 518–529, 2015.

[13] R. Qin, A. Zhou, and D. Lau, "Effect of reinforcement ratio on the flexural performance of hybrid FRP reinforced concrete beams," *J Composites Part B*, vol. 108, pp. 200-209, 2017.

[14] H. O. A. Said, M. A. M. Hassanean, Y. A. Hassanean, and A. M. A. Ibrahim, "Flexural behavior of concrete box girders reinforced with mixed steel and basalt fiber-reinforced polymer," *J Engineering Sciences*, vol. 51, pp. 223-241, 2023.

[15] C. Aksoylu, S. Yazman, Y. O. Özkılıç, L. Gemi, and M. H. Arslan, "Experimental analysis of reinforced concrete shear deficient beams with circular web holes strengthened by CFRP composite," *J Composite Structures*, vol. 249, pp. 112561, 2020.

[16] B. H. Osman, E. Wu, B. Ji, and A. M. S. Abdelgader, "A state of the art review on reinforced concrete beams with holes retrofitted with FRP," *Int J Adv Struct Eng*., vol. 8, pp. 253-267, 2016.

[17] Q. M. Shakir, "Non-linear analysis of high strength reinforced concrete beams with large holes," *Jordan J Civil Eng*., vol. 10:pp. 451-461, 2016.

[18] B. Aykac, S. Aykac, I. Kalkan, B. Dundar, and H. Can, "Flexural behavior and strength of reinforced concrete beams with multiple transverse holes," *J ACI Struct*., vol. 111, pp. 267-278, 2014.

[19] B. Aykac, I. Kalkan, S. Aykac, and Y. E. Egriboz, "Flexural behavior of RC beams with regular square or circular web holes," *J Eng Struct*., vol. 56, pp. 2165–2174, 2013.

[20] A. M. Abdel-Hafez, "Behaviour of reinforced high-strength concrete beams with holes subjected to static and repeated loadings," *J Eng Sci*., vol. 37, pp. 1343–1358, 2009.

[21] K. H. Yang, H. C. Eun, and H. S. Chung, "The influence of web holes on the structural behavior of reinforced high-strength concrete deep beams," *J Eng Struct*., vol. 28, pp. 1825-1834, 2006.

[22] M. Mansur, K. H. Tan, and W. Weng, "Analysis of concrete beams with circular web holes using strut-and-tie models," *Malaysian J Civil Eng*., vol. 18, 2006.
DOI: https://doi.org/10.11113/mjce.v18.15733.

[23] M. Mansur and K. H. Tan, "Concrete beams with holes: analysis and design," *CRC Press*., 1999.

[24] H. K. Tan and M. A. Mansur, "Design procedure for reinforced concrete beams with large web holes," *J Struct*., vol. 93, pp. 404-411, 1996.

[25] M. A. Mansur, L. M. Huang, K. H. Tan, and S. Lee, "Deflections of reinforced concrete beams with web holes," *J ACI Struct*., vol. 4, pp. 391-397, 1992.

[26] M. Mansur, Y. Lee, K. Tan, and S. Lee, "Tests on RC continuous beams with holes," *J Struct Eng*., vol. 117, pp. 593-606, 1991.

[27] S. S. Pillai and A. Johny, "Analytical study on shear behavior of reinforced concrete beam with varying shapes of web hole," *International Journal of Engineering Research & Technology (IJERT)*, vol. 6, pp. 1-4, 2018.

[28] O. M. Ramadan, K. G. Metwally, and W. M. Shaban, "Proposed recommendations for the design of reinforced concrete beams with holes," *World conference on Advances in Structural Engineering and Mechanics* (ASEM15) Incheon, Korea, 2015.

[29] O. M.O. Ramadan, S. K. Elwan, and A. M. Ahmed, "Effect of transverse rectangular holes on the behavior of reinforced concrete beams having various percentages area of steel," *Proc. of the Thirteenth International Conference on Structural and Geotechnical Engineering, 13ICSGE, Cairo, Paper No. RCS-021,* 2009.

[30] S. Amiri and R. Masoudnia, "Investigation of the hole effects on the behavior of concrete beams without additional reinforcement in hole region using FEM method," *Australian J Basic and Applied Sciences*, vol. 5, pp. 617-627, 2011.

[31] M. Mansur, "Effect of holes on the behaviour and strength of R/C beams in shear," *J Cem Concr Compos*., vol. 20, pp. 477-486, 1998.

[32] F. El Ame, J. N. Mwero, and C. K. Kabubo, "Holes effect on the performance of reinforced concrete beams loaded in bending and shear," *J Engineering, Technology & Applied Science Research*, vol. 10, pp. 5352-5360, 2020.

[33] A. Altalmas, A. El Refai, and F. Abed, "Bond degradation of basalt fiber-reinforced polymer (BFRP) bars exposed to accelerated aging conditions," *J Construction and Building Materials*, vol. 81, pp. 162-171, 2015.

[34] A. M. A. Ibrahim, M. F. M. Fahmy, and Z. Wu, "3D finite element modeling of bond controlled behavior of steel and basalt FRP-reinforced concrete square bridge columns under lateral loading," *J Composite Structures*, vol. 143, pp. 33-52, 2016.

[35] A. M. A. Ibrahim, Z. Wu, M. F. M. Fahmy, and D. Kamal, "Experimental study on cyclic response of concrete bridge columns reinforced by steel and basalt FRP reinforcements," *J Compos. Constr*., vol. 20, pp. 04015062, 2016.

[36] S. Yehia, A. M. A. Ibrahim, and B. Faihan, "Experimental study on steel-FRP reinforced concrete beams with large rectangular holes." *International J. Scientific & Engineering Research,* vol. 12, pp. 657-661, 2021.

[37] S. Yehia, B. Faihan, and A. M. A. Ibrahim, "Strength of Hybrid Steel-BFRP Reinforced Concrete Beams with Openings in the D-Region Strengthened Internally and Externally," *J. Buildings*, vol. 13, pp. 2522, 2023.

[38] ANSYS – Release Version 15.0, "A finite element computer software and user manual for nonlinear structural analysis," *Canonsburg, USA*, 2013.

[39] ACI:440.3R-12; Guide Test Methods for Fiber-Reinforced Polymer (FRP) Composites for Reinforcing or Strengthening Concrete and Masonry Structures. American Concrete Institute Committee Report. *American Concrete Institute Committee: Farmington Hills, MI, USA, 2012*.

[40] ACI CODE-318-19(22); Building Code Requirements for Structural Concrete and Commentary (Reapproved 2022). *American Concrete Institute: Farmington Hills, MI, USA, 2022.*

[41] S. A. A. Mustafa and H. A. Hassan, "Behavior of concrete beams reinforced with hybrid steel and FRP composites," *HBRC Journal*, vol. 14, pp. 300-308, 2018.

[42] A. M. A. Ibrahim, H. A. Diab, Y. A. Hassanean, O. A. Farghal, and M. M. a. Ismail, "Numerical study on the behavior and strength of concrete beam strengthening with fiber reinforced concrete jackets," *J. Structures*, vol. 50, pp. 1557-1572, 2023.

[43] J. G. MacGregor, "Reinforced concrete mechanics and design," *Englewood Cliffs, NJ: Prentice-Hall Inc,* 1992.

[44] K. J. Willam and E. P. Warnke, "Constitutive models for the triaxial behavior of concrete," *IABSE Proceedings,* No. *19*, pp. *1-30*, 1975.

[45] D. Kachlakev, T. Miller, and S. Yim, "Finite element modeling of reinforced concrete structures strengthened with FRP laminates," *Oregon Dept. of Transp., USA, Res. Group, Final Report SPR, 316*, 2001.

[46] A. M. A. Ibrahim, M. F. M. Fahmy, and Z. Wu, "Numerical simulation on fracturing bond mechanisms of different basalt FRP bars," *J Applied Mechanics*, vol. 71, pp. 289-298, 2015.

[47] CEB. (1992). CEB-FIP Model Code 90. *London*.